Effect of high pressure on charge density wave formation and magnetic structure in the cubic high-pressure phase of TbGe$_{2.85}$

D. A. Salamatin

Vereshchagin Institute for High Pressure Physics, RAS, 142190 Moscow, Russia;
Department of Problems of Physics and Energetics, Moscow Institute of Physics and Technology, 141700 Dolgoprudny, Russia;
and Dzelepov Laboratory of Nuclear Problems, Joint Institute for Nuclear Research, 141980 Dubna, Russia

V. A. Sidorov

Vereshchagin Institute for High Pressure Physics, RAS, 142190 Moscow, Russia
and Department of Problems of Physics and Energetics, Moscow Institute of Physics and Technology, 141700 Dolgoprudny, Russia

S. E. Kichanov and D. P. Kozlenko

Frank Laboratory of Neutron Physics, Joint Institute for Nuclear Research, 141980 Dubna, Russia

L. N. Fomicheva

Vereshchagin Institute for High Pressure Physics, RAS, 142190 Moscow, Russia

A. V. Nikolaev

Skobeltsyn Institute of Nuclear Physics Lomonosov Moscow State University, 119991 Moscow, Russia
and Department of Problems of Physics and Energetics, Moscow Institute of Physics and Technology, 141700 Dolgoprudny, Russia

O. L. Makarova

Kurchatov's Complex of NBICS-technologies, National Research Center "Kurchatov Institute", 123182 Moscow, Russia

A. V. Tsvyashchenko[*]

Vereshchagin Institute for High Pressure Physics, RAS, 142190 Moscow, Russia
and Skobeltsyn Institute of Nuclear Physics Lomonosov Moscow State University, 119991 Moscow, Russia

In this paper the charge density wave (CDW) and magnetic ordering for the high-pressure phase of TbGe$_{2.85}$ with the AuCu$_3$ structure have been studied by means of electrical resistivity and neutron powder diffraction at pressures up to 3 and 5 GPa, respectively. The electrical resistivity measurements showed that the charge density wave transition temperature T_{CDW} decreases with increasing the external pressure and the CDW transition in TbGe$_{2.85}$ is suppressed at $P \geqslant 2.6$ GPa. The Néel temperature T_N is approximately independent of the pressure. The neutron powder diffraction at low temperatures and high pressures reveals the appearance of the second magnetic commensurate phase at $P = 1.2$ GPa with wave-vector $\mathbf{k} = (1/2,0,0)$. The calculation of the electronic structure of the TbGe$_3$ (AuCu$_3$-type structure) compound was also performed. The high value of the electronic states at the Fermi level confirms the instabilities of the stoichiometric compound TbGe$_3$.

I. INTRODUCTION

Recently, the question about the formation of the charge density wave (CDW) in intermetallic compounds has drawn new interest, especially in relation with the superconductivity or/and magnetic structure. The charge density wave is a spatial modulation of the density of conduction electrons. Usually the CDW is formed in low-dimensional systems (quasione dimensional and quasitwo dimensional) [1]. CDW can also arise in three-dimensional systems [2–5]. Besides that, it is observed in superconductors [3,6].

It is commonly assumed that the crucial factor in CDW formation is the Fermi-surface nesting [1,7]. The nesting of the Fermi surface arises when large fragments of the Fermi surface are parallel to each other in reciprocal space. In other words, one fragment of the Fermi surface can be translated to another fragment by vector **Q**. The Fermi-surface nesting produces the divergence or a local maximum in the real part of the electronic susceptibility function $\chi(\mathbf{q},\omega)$ for $\mathbf{q} = \mathbf{Q}$, which determines the instability of the electronic system (CDW) [7].

However, recent experimental and theoretical data collected for different compounds with CDW transition show that in many cases the Fermi-surface nesting is not the main factor in CDW formation [7,8]. Therefore, synthesis and studying of novel compounds with the CDW can be helpful in our better understanding of all mechanisms responsible for CDW formation.

Another much debated problem in solid-state physics is the competition between CDW and magnetic ordering. It is known that the Fermi-surface nesting with wave-vector $\mathbf{q}_{nest}$ can drive a magnetic structure with the same wave vector [9].

*tsvyash@hppi.troitsk.ru

In some rare-earth-based compounds, it has been shown that the ferromagnetic ordering of rare-earth moments ($SmNiC_2$) completely suppresses the CDW [10], whereas the antiferromagnetic (AFM) one ($NdNiC_2$, $Er_5Ir_4Si_{10}$) suppresses the CDW only partially [11,12]. Although the precise mechanism of the relation between the CDW and the magnetic properties is currently under debate, in Ref. [11] a simple assumption about this coupling is put forward. It is based on the mechanism of the pair electron interaction when the CDW and FM/AFM structures are formed.

Many rare-earth compounds with the $AuCu_3$ structure and the $Pm\bar{3}m$ space group (No. 221) have commensurate AFM structures. For example, $TmGa_3$ [13]; $ErPd_3$, $TmPd_3$ [14]; RIn_3 (where $R =$ Nd, Tb, Dy, Ho, and Er) [15]; RSn_3 ($R =$ Sm, Eu, and Gd) [16] are characterized by wave vectors belonging to the star $\langle 1/2,0,0\rangle$ or $\langle 1/2,1/2,0\rangle$. However, despite the simple crystallographic structure, some compounds have incommensurate magnetic structures. For example, in $TbPd_3$ an incommensurate AFM helical structure has been found ($T_N \approx 4$ K) [14]. In $ErGa_3$ the incommensurate magnetic order was described by the wave-vector $\mathbf{k} = (1/2 + \tau,1/2,0)$, where $\tau = 0.042$ [17]. In $NdIn_3$ the magnetic moments also were found to be rectangularly modulated with the periodicity, incommensurate with the crystallographic order [18].

In this paper we discuss the interplay between the CDW and the magnetic ordering for the high-pressure phase of $TbGe_{2.85}$ which has the $AuCu_3$ structure [19]. Temperature dependencies of the electrical resistivity, heat capacity, and magnetic susceptibility reported earlier in Ref. [20] have shown two peculiarities. The first peculiarity at $T_{CDW} = 145$ K was related with the charge density wave transition, whereas the second at $T_N = 19$ K was related with AFM transition. Time different perturbed angular correlations measurements showed that the CDW modulation period becomes commensurate (locks in) below $T = 19$ K. On the other hand, the neutron diffraction at 10 K indicated that the AFM structure is an incommensurate helix with the wave-vector $\mathbf{k} = (1/2,0,0.165)$.

It was suggested [20] that the CDW suppresses the local inversion center in $TbGe_{2.85}$ and the $AuCu_3$ cubic phase transforms into a "quasicubic" structure (i.e., without the inversion center). This leads to the appearance of a finite Dzyaloshinskii-Moriya interaction (DMI). The antisymmetric exchange DMI results the spin canting and the formation of an incommensurate antiferromagnetic helical structure below 19 K at ambient pressure.

The temperature dependence of electrical resistivity indicated the appearance of the CDW at $T = 14.3$ K in $TbPd_3$. This confirms the assumption of the relation of the CDW with an incommensurate magnetic structure in $TbPd_3$ [20].

In the present paper we study the CDW and the magnetic structure of $TbGe_{2.85}$ further by considering the effect of external pressure. In Ref. [20] it has been shown that the application of 0.9 GPa led to a decrease in the CDW temperature. The same behavior was observed for example in work by D. A. Zocco *et al.* [21]. Here we will show that the external pressure suppresses the CDW state making the magnetic structure of $TbGe_{2.85}$ commensurate. In addition, we present *ab initio* calculations of the electronic structure of $TbGe_3$.

II. EXPERIMENT AND THEORY

Polycrystalline samples of $TbGe_{2.85}$ were synthesized at a pressure of 8 GPa as described in Ref. [19].

The crystal structure was examined by x-ray diffraction [19] and neutron powder diffraction [20] at normal temperature and ambient pressure. The refinements of the diffraction data have shown that the polycrystalline samples of $TbGe_{2.85}$ have the $AuCu_3$-type structure [$Pm\bar{3}m$ space group (No. 221)] with the lattice constant $a = 4.287$ Å at $T = 300$ K.

The electrical resistivity was measured by the four-probe method. The sample and the pressure sensor (Pb) were placed in a teflon ampoule filled with a pressure-transmitting liquid. The clamped toroid-type cell was used to generate high pressures [22].

Neutron powder-diffraction measurements at high pressures up to 5.1 GPa were performed at low temperatures with the DN-12 spectrometer [23] at the IBR-2 high-ux pulsed reactor [Frank Laboratory of Neutron Physics, Joint Institute for Nuclear Research, Dubna, Russia] using the sapphire anvil high-pressure cell [24]. A neutron beam passed through one anvil of the high-pressure cell and scattered on the sample. The detector ring at $90°$ collected the scattered neutrons that passed through the aluminum gasket but the level of absorption was low. The diameter of the gasket was $D = 4$ mm, the thickness of the plate was 0.8 mm, and the sample hole was 2.2 mm.

The scattered neutrons detected at $45.5°$ passed through the sapphire anvil, not through the gasket. The wavelength depended absorption in single-crystal sapphire was low [25].

The pressure was determined by the ruby fluorescence technique. Diffraction patterns were collected at scattering angles of $45.5°$ and $90°$ with the resolutions $\Delta d/d = 0.022$ and 0.015, correspondingly.

Spectra from different detectors were collected and summed. The final pattern was normalized on the initial beam profile, which was the vanadium spectrum. The sample background was considered small in comparison with the background of the empty pressure cell and environment. Experimental data of the neutron powder-diffraction experiments were analyzed by the Rietveld method using the FULLPROF software [26].

The calculations of the electronic structure of $TbGe_3$ were performed using the FLAPW-MOSCOW program [27]. The program realizes the linearized augmented plane-wave method with the potential of the general shape for calculations of solids including semicore electron states [28]. For $TbGe_3$ 257 plane-wave basis functions were used determined by the cutoff parameter $R_{MT}^{max} K_{max} = 9$. The $5p$(semicore) $+ 6s4f$ electron shells of terbium and the $4s4p$ electron shells of germanium were treated as valence electron shells. The spin-orbit interaction was taken into account as a perturbation.

III. EXPERIMENTAL AND THEORETICAL RESULTS

Temperature dependencies of electric resistivity $\rho(T)$ for $TbGe_{2.85}$ at different pressures are shown in Fig. 1. The temperature of the CDW formation was determined from the condition of the minimum of $d\rho/dT$ as a function of temperature. Transition at T_{CDW} becomes broader with increasing the pressure. In the paper [29] a similar broadening for $NbSe_3$ was
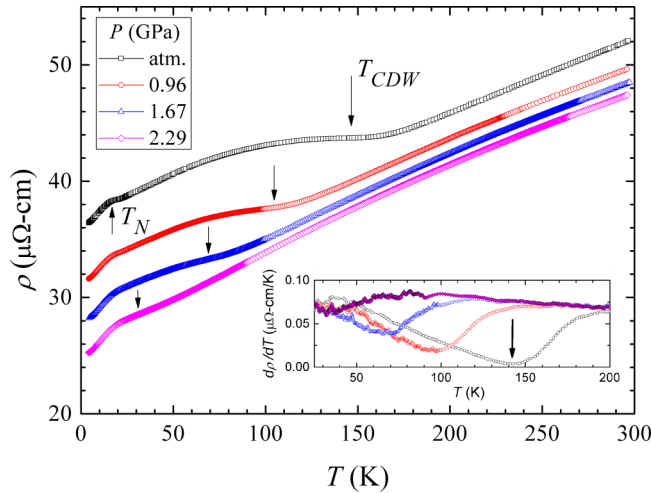
FIG. 1. Resistivity of $TbGe_{2.85}$ versus temperature at different external pressures. The arrows indicate the temperatures of the CDW and antiferromagnetic transitions. The inset: Plots of $d\rho/dT$ versus temperature used for the determination of the CDW transition temperature.

associated with fluctuations. With the application of pressure, the temperature of the CDW transition decreases with the speed of $dT_{CDW}/dP \approx -48$ K/GPa (the dependence is not strictly linear) and vanishes at $P \approx 2.6$ GPa. In this pressure region the Néel temperature exhibits a weak linear dependence $dT_N/dP = 1.7$ K/GPa (see Fig. 2).

The neutron powder diffraction of $TbGe_{2.85}$ has been measured at various pressures (P) and temperatures (T): at $P = 1.2$ GPa (for $T = 300$, 18, and 10 K), at 3.1 GPa (for 200 and 10 K), and at 5.1 GPa (for 10 K). The obtained diffractograms and their refinements are shown in Fig. 3. The refinement of the magnetic peaks of the diffraction patterns
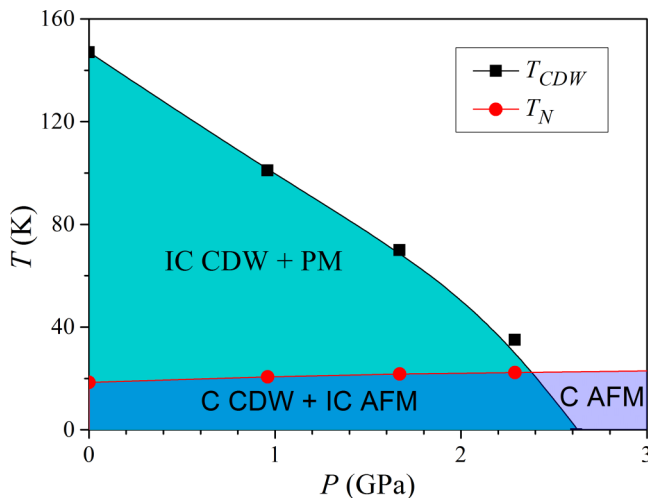
FIG. 2. Antiferromagnetic transition temperature T_N (red points and line) and CDW transition temperature T_{CDW} (black squares and line) of $TbGe_{2.85}$ versus pressure. The colors indicate different magnetic and structural phases (IC stands for the incommensurate CDW phase, C stands for the commensurate CDW phase, PM stands for the paramagnetic phase, and AFM stands for the antiferromagnetic phase).
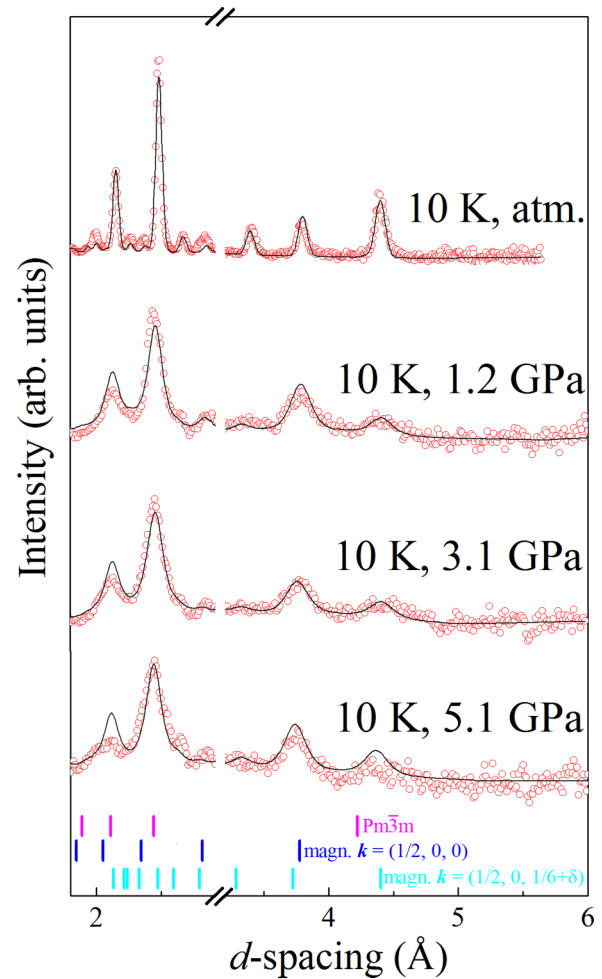
FIG. 3. Refined neutron powder-diffraction patterns of $TbGe_{2.85}$. Experimental points (red points) and calculated profiles (black lines) are shown. Tick marks at the bottom represent the calculated positions of nuclear peaks for the $Pm\bar{3}m$ space group (upper row, pink color) and magnetic peaks for the commensurate phase with wave-vector $\mathbf{k}_1 = (1/2,0,0)$ (medium row, blue color) and the incommensurate phase with wave-vector $\mathbf{k}_2 = (1/2,0,1/6 + \delta)$ (lower row, turquoise color).

was performed for two different magnetic structures: the first with commensurate wave-vector $\mathbf{k}_1 = (1/2,0,0)$ and the magnetic moments $\mu_{Tb} \approx 9.3\mu_B$ of Tb ions directed along the [1, 0, 0] direction and the second with incommensurate wave-vector $\mathbf{k}_2 = (1/2,0,1/6 + \delta)$, lying close to the value given in Ref. [20]. Here δ is an incommensurability parameter, which slightly increases with pressure. We have not observed a symmetry change in the $AuCu_3$ crystallographic structure found at normal conditions in paramagnetic or magnetically ordered states of $TbGe_{2.85}$ under pressure, so we found no structural modulations in the CDW state. However, probably the pressure induces the appearance of crystallographic texture. The lattice constant slightly decreases with pressure. We have also performed x-ray diffraction at room temperature of $TbGe_{2.85}$ after releasing the external pressure. No difference with the diffraction data reported in Ref. [19] has been found.

Figure 4 presents the suppression of the intensity of the magnetic peak of the incommensurate magnetic structure of $TbGe_{2.85}$ under pressure.
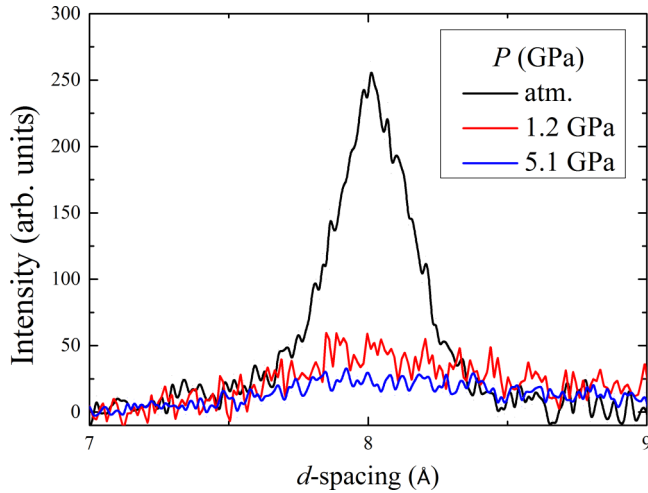
FIG. 4. The intensity of the $(0,0,0) + \mathbf{k}_2$ magnetic peak versus the interplanar d spacing at 10 K.

The results of *ab initio* electron band-structure calculations of TbGe$_3$ taking into account the spin-orbit coupling are shown in Figs. 5 and 6. The partial occupation of the $4f$ states at the Tb site is 8.51. The Fermi level is found to lie in a very narrow
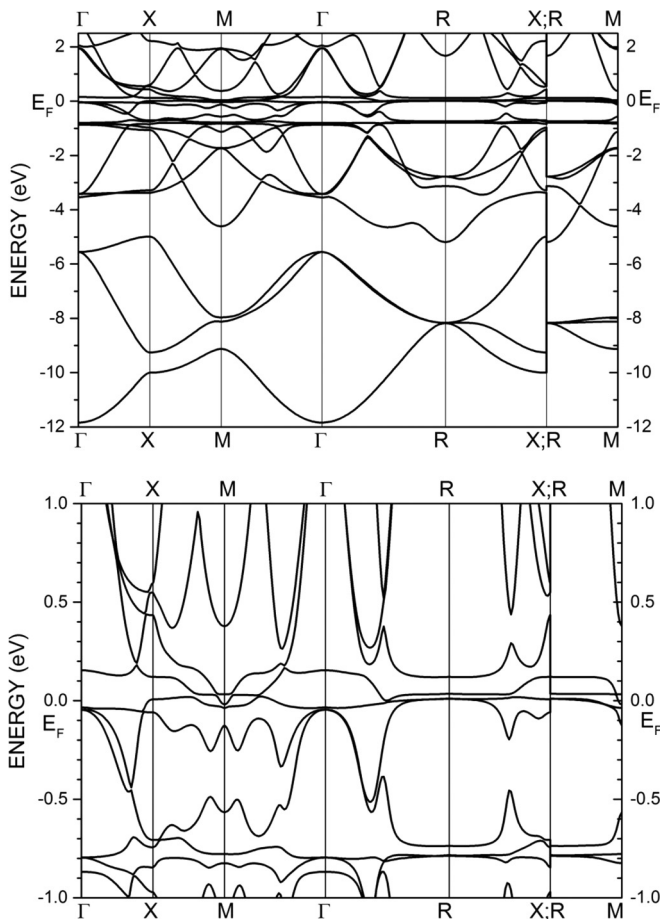
FIG. 5. The electron band structure of TbGe$_3$ along high-symmetry directions. Upper panel: in the $4s$(Ge)$4p$(Ge)$4f$(Tb) valence-band energy region; lower panel: in the vicinity of the Fermi energy. The Fermi level corresponds to the zero energy.
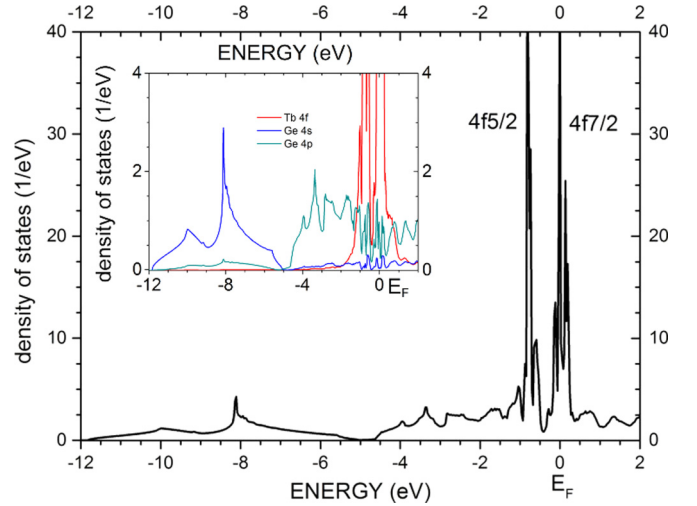
FIG. 6. The density of states (DOS) of TbGe$_3$ versus energy ($E_F = 0$). The inset: partial DOS of $4s,4p$ states of Ge and $4f$ states of Tb with a magnified scale.

peak of the density of the $4f_{7/2}$ states of Tb (see Fig. 6), which results in the very large density of states at the Fermi energy $n(E_F) = 58.8$ states/eV. The main partial contribution to this value is due to the $4f_{7/2}$ levels of Tb (95%). The $4f$ states can clearly be seen in the band structure (see Fig. 5). They are distinguished by approximately horizontal (nondispersive) electron bands. An abnormally high value of $n(E_F)$ implies an instability of the electron structure of this compound, which is confirmed by experimental magnetic and structure changes discussed in the present paper. Both structural and magnetic transitions lead to a decrease in the value of $n(E_F)$, thereby effectively reducing the degeneracy of electron states near the Fermi level. Another feature of the density-of-state plot clearly seen in Fig. 6 is the minimum of the density of states around -5 eV, which corresponds to the separation of s- and p-electron bands of germanium. The separation between these bands can also be found between -8 and -4 eV in the band-structure plot in Fig. 5. Notice that in correspondence with the space symmetry there are no quadrupole components of the full potential at the terbium, but they are allowed at the sites of germanium. The calculated electric-field gradient (EFG) at the Ge site is $V_{zz} = 11.4 \times 10^{17}$ V/sm^2. This value is about five times larger than the EFG measured experimentally [20] in TbGe$_{2.85}$. The difference is accounted for by the fact that the experimental compound is nonstoichiometric and that the experimental value of the EFG is obtained at probe ^{111}Cd atoms inserted in the Ge sublattice. In comparison with the Ge atom, the Cd probe having completely filled the d and s shells is expected to experience only a reduced quadrupolar component (and EFG) of the crystal potential.

IV. DISCUSSION

From Figs. 1 and 2 for the temperature data of the electrical resistivity of TbGe$_{2.85}$ at various pressures it follows that the CDW transition temperature decreases with applied pressure and the CDW peculiarity at the temperature dependence of electrical resistivity is absent if the external pressure is above $P = 2.6$ GPa. We then conclude that the CDW sets in under

applied pressures below $P = 2.6$ GPa while the temperature of the CDW transition $T_{CDW}(P)$ decreases with pressure. To investigate the change in the magnetic structure of TbGe$_{2.85}$ with applied pressures after the suppression of the CDW transition, the neutron powder diffraction has been carried out (Figs. 3 and 4). The refinement of neutron powder-diffraction data shows that already at $P = 1.2$ GPa the incommensurate magnetic structure with the wave-vector $\mathbf{k}_2 = (1/2,0,1/6 + \delta)$ is partially suppressed. This finding is further supported by the $d \approx 8$-Å magnetic peak data given in Fig. 4, whose intensity decreases with pressure. Notice also that at high pressures new magnetic peaks appear, which can be indexed with the wave-vector $\mathbf{k}_1 = (1/2,0,0)$. (The peaks are absent at $P = 3.1$ GPa and $T = 200$ K.) This indicates that at $P > 1.2$ GPa and $T < T_N$, in TbGe$_{2.85}$ two different magnetic phases are formed: The first is the incommensurate phase with the wave vector close to the vector found at atmospheric pressure, and the second is the commensurate phase with the wave-vector $\mathbf{k}_1 = (1/2,0,0)$, which is typical for the RSn$_3$ compounds with the AuCu$_3$ structure [30]. (It is worth mentioning that the Néel temperature T_N demonstrates a weak continuous growth with increasing pressure, Fig. 2.) We assume that the suppression of the CDW effectively enables the inversion symmetry in TbGe$_{2.85}$ broken by the CDW, which leads to the disappearance of the asymmetric interaction of Dzyaloshinsky-Moria responsible for the incommensurate magnetic structure [20]. However, we were not able to estimate accurately the ratio between the volume of the commensurate high-pressure phase and the volume of the incommensurate magnetic structure which is realized at normal pressure. This is partly due to a large width of the diffraction peaks, Fig. 3. The broadening of the diffraction peaks can be caused by several reasons. In our case deformations arise from the effect of nonhydrostaticity of pressure in the neutron-diffraction experiment, which amounts to $\pm 15\%$ [31]. Second, under external pressure vacancies in the Ge sites of the nonstoichiometric TbGe$_{2.85}$ compound result in inhomogeneous strains and lead to a high background

level of the diffraction pattern [32]. The results of electron band-structure calculations for TbGe$_3$ (Figs. 5 and 6) show that the Fermi level lies in a narrow peak of the density of the $4f_{7/2}$ states of Tb, which leads to the high value of the density of states at the Fermi energy $n(E_F) = 58.8$ states/eV. This is an indication of the structural instability of TbGe$_3$ which manifests itself in the formation of the nonstoichiometric composition of TbGe$_{2.85}$ and the charge density wave. The measured EFG in TbGe$_{2.85}$ at $T = 4$ K is smaller in order in comparison with the calculated EFG in TbGe$_3$ [20]. This fact can be related with the high value of DOS at the Fermi level $n(E_F)$.

V. CONCLUSIONS

The formation of the charge density wave in the high-pressure cubic phase of TbGe$_{2.85}$ is suppressed by external pressure. The observed pressure suppression of the CDW is accompanied by the change in the magnetic structure from incommensurate to commensurate at $P \geqslant 1.2$ GPa. The similar magnetic structure with wave-vector $\mathbf{k} = (1/2,0,0)$ is observed in the RSn$_3$ compounds without the CDW. It is conceivable that this behavior of the magnetic order is related with the transition from a quasicubic structure to the AuCu$_3$ cubic structure with a center of inversion. The instability of the cubic phase of the stoichiometric TbGe$_3$ compound (the AuCu$_3$ lattice) is associated with a high density of states at the Fermi energy level formed by the f electrons.

[1] G. Grüner, *Density Waves in Solids* (Addison-Wesley, Reading, MA, 1994).

[2] R. Tediosi, F. Carbone, A. B. Kuzmenko, J. Teyssier, D. van der Marel, and J. A. Mydosh, Phys. Rev. B **80**, 035107 (2009).

[3] S. Gerber, H. Jang, H. Nojiri, S. Matsuzawa, H. Yasumura, D. A. Bonn, R. Liang, W. N. Hardy, Z. Islam, A. Mehta *et al.*, Science **350**, 949 (2015).

[4] R. M. Fleming, F. J. DiSalvo, R. J. Cava, and J. V. Waszczak, Phys. Rev. B **24**, 2850 (1981).

[5] Y. Singh, R. Nirmala, S. Ramakrishnan, and S. K. Malik, Phys. Rev. B **72**, 045106 (2005).

[6] H.-F. Zhai, Z.-T. Tang, H. Jiang, K. Xu, K. Zhang, P. Zhang, J.-K. Bao, Y.-L. Sun, W.-H. Jiao, I. Nowik *et al.*, Phys. Rev. B **90**, 064518 (2014).

[7] M. D. Johannes and I. I. Mazin, Phys. Rev. B **77**, 165135 (2008).

[8] X. Zhua, Y. Caoa, J. Zhangb, E. W. Plummerb, and J. Guoa, Proc. Natl. Acad. Sci. U.S.A. **112**, 2367 (2015).

[9] O. K. Andersen and T. L. Loucks, Phys. Rev. **167**, 551 (1968).

[10] S. Shimomura, C. Hayashi, G. Asaka, N. Wakabayashi, M. Mizumaki, and H. Onodera, Phys. Rev. Lett. **102**, 076404 (2009).

[11] N. Yamamoto, R. Kondo, H. Maeda, and Y. Nogami, J. Phys. Soc. Jpn. **82**, 123701 (2013).

[12] F. Galli, R. Feyerherm, R. W. A. Hendrikx, E. Dudzik, G. J. Nieuwenhuys, S. Ramakrishnan, S. D. Brown, S. van Smaalen, and J. A. Mydosh, J. Phys.: Condens. Matter **14**, 5067 (2002).

[13] P. Morin, M. Giraud, P. L. Regnault, E. Roudaut, and A. Czopnik, J. Magn. Magn. Mater. **66**, 345 (1987).

[14] O. Elsenhans, P. Fischer, A. Furrer, K. N. Clausen, H. G. Purwins, and F. Hulliger, Z. Phys. B: Condens. Matter **82**, 61 (1991).

[15] R. M. Galera and P. Morin, J. Magn. Magn. Mater. **116**, 159 (1992).

[16] M. Shafiq, I. Ahmad, and S. J. Asadabadi, J. Appl. Phys. **116**, 103905 (2014).

[17] A. Murasik, A. Czopnik, L. Keller, and P. Fischer, J. Magn. Magn. Mater. **213**, 101 (2000).

[18] S. Mitsuda, P. M. Gehring, G. Shirane, H. Yoshizawa, and Y. Onuki, J. Phys. Soc. Jpn. **61**, 1469 (1992).

[19] A. V. Tsvyashchenko, A. I. Velichkov, A. V. Salamatin, L. N. Fomicheva, D. A. Salamatin, G. K. Ryasny, A. V. Nikolaev, M. Budzynski, R. A. Sadykov, and A. V. Spasskiy, J. Alloys Compd. **552**, 190 (2013).

[20] A. V. Tsvyashchenko, D. A. Salamatin, V. A. Sidorov, A. E. Petrova, L. N. Fomicheva, S. E. Kichanov, A. V. Salamatin, A. Velichkov, D. R. Kozlenko, A. V. Nikolaev, G. K. Ryasny, O. L. Makarova, D. Menzel, and M. Budzynski, Phys. Rev. B **92**, 104426 (2015).

[21] D. A. Zocco, J. J. Hamlin, K. Grube, J.-H. Chu, H.-H. Kuo, I. R. Fisher, and M. B. Maple, Phys. Rev. B **91**, 205114 (2015).

[22] A. E. Petrova, V. A. Sidorov, and S. M. Stishov, Physica B **359-361**, 1463 (2005).

[23] V. L. Aksenov, A. M. Balagurov, V. P. Glazkov, D. P. Kozlenko, I. V. Naumov, B. N. Savenko, D. V. Sheptyakov, V. A. Somenkov, A. P. Bulkin, V. A. Kudryashev, and V. A. Trounov, Physica B **265**, 258 (1999).

[24] V. P. Glazkov and I. N. Goncharenko, Fiz. Tekh. Vysokih Davlenij **1**, 56 (1991) (in Russian).

[25] A. V. Rutkayskas, D. P. Kozlenko, S. E. Kichanov, G. D. Bokuchava, E. V. Lukin, and B. N. Savenko, J. Surf. Invest.: X-ray, Synchrotron Neutron Tech. **9**, 317 (2015).

[26] J. Rodriguez-Carvajal, Physica B **192**, 55 (1993).

[27] The FLAPW-MOSCOW code [registration number 2015616990 (Russia) from 26 June 2015], see also A. V. Nikolaev, I. T. Zuraeva, G. V. Ionova, and B. V. Andreev, Phys. Solid State **35**, 213 (1993).

[28] A. V. Nikolaev, D. Lamoen, and B. Partoens, J. Chem. Phys. **145**, 014101 (2016).

[29] S. Yasuzuka, K. Murata, T. Fujimoto, M. Shimotori, and K. Yamaya, J. Phys. Soc. Jpn. **74**, 1782 (2005).

[30] A. Benidris, A. Zaoui, M. Belhadj, M. Djermouni, and S. Kacimi, J. Supercond. Nov. Magn. **28**, 2215 (2015).

[31] D. P. Kozlenko, N. T. Dang, S. E. Kichanov, E. V. Lukin, A. M. Pashayev, A. I. Mammadov, S. H. Jabarov, L. S. Dubrovinsky, H.-P. Liermann, W. Morgenroth *et al.*, Phys. Rev. B **92**, 134409 (2015).

[32] J. D. Makinson, J. S. Lee, S. H. Magner, R. J. De Angelis, W. N. Weins, and A. S. Hieronymus, *Denver X-Ray Conference (DXC) on Applications of X-Ray Analysis, Denver, 2000* (ICDD, Newton Square, PA, 2000).